Impact of Trailing Edge Serrations on Aeroacoustic Performance

[1]Vattikula Sai Ram, [2]Seetha Rajesh, [3]G. Sravanthi

[1]Student, [2]Student, [3]Assistant Professor
[1]Department of Aeronautical Engineering
[1]Institute of Aeronautical Engineering, Hyderabad, India
[1]vattikulasairam021@gmail.com, [2]rajeshseetha26@gmail.com, [3]g.sravanthi@iare.ac.in

Abstract— **This study investigates the aerodynamic and aeroacoustic performance of a NACA 2412 airfoil with trailing edge serrations using a computational approach. A three-dimensional model is analyzed at an angle of attack of 5° and a freestream velocity of 45 m/s. The flow field is simulated using the SST k–ω turbulence model, and far-field noise is predicted using the Ffowcs Williams–Hawkings (FW-H) acoustic analogy. The results for the serrated configuration are compared with a baseline airfoil to evaluate the impact of geometric modification. Aerodynamic analysis shows a slight increase in drag and a marginal reduction in lift for the serrated case. However, aeroacoustic results indicate a consistent broadband noise reduction across multiple receiver locations, with noticeable improvements in the low-to-mid frequency range. The findings suggest that trailing edge serrations effectively reduce noise by altering flow structures near the trailing edge while maintaining acceptable aerodynamic performance.**

Keywords— **Trailing edge serrations, Aeroacoustics, NACA 2412 airfoil, Sound pressure level (SPL), Computational fluid dynamics (CFD), SST k–ω model, FW-H acoustic analogy, Noise reduction.**

I. Introduction

The increasing use of aircraft and wind turbines has made aerodynamic noise an important concern, especially in areas close to human activity. Apart from affecting human comfort, this noise can also have environmental impacts, which makes its reduction an important objective in modern aerodynamic design [1].

Aerodynamic noise is mainly generated due to the interaction between turbulent flow and solid surfaces. Among the different sources, trailing edge noise is considered one of the dominant contributors in subsonic flows. This type of noise occurs when turbulent boundary layer fluctuations interact with the sharp trailing edge of an airfoil, producing broadband acoustic emissions due to unsteady pressure variations [2].

To reduce this noise, several passive control methods have been proposed. One of the most promising approaches is the use of trailing edge serrations, inspired by the silent flight characteristics of owls. These serrations modify the flow near the trailing edge by disturbing the coherence of turbulent structures, which leads to a reduction in pressure fluctuations and, consequently, noise generation [3].

Over the years, both experimental and numerical studies have shown that serrations can effectively reduce noise levels without significantly affecting aerodynamic performance. Experimental investigations on serrated airfoils have reported noticeable reductions in sound pressure levels due to changes in flow behavior near the trailing edge [4].

With the advancement of computational methods, numerical simulations based on Computational Fluid Dynamics (CFD) have become widely used to study aeroacoustic behavior. When combined with acoustic models such as the Ffowcs Williams–Hawkings (FW-H) equation, these methods allow prediction of far-field noise based on unsteady flow data obtained from simulations [2][5].

More recent studies using advanced turbulence models, such as Large Eddy Simulation (LES), have provided deeper insight into the noise reduction mechanism. These studies indicate that serrations reduce the spanwise correlation of turbulent structures and alter vortex dynamics near the trailing edge, leading to a reduction in sound pressure levels [1][6].

In addition, the effectiveness of serrations depends strongly on their geometric parameters, such as amplitude and wavelength. Different configurations can lead to varying levels of noise reduction, highlighting the importance of proper design optimization [7].

Therefore, the present study aims to investigate the impact of trailing edge serrations on aeroacoustic performance by comparing a baseline airfoil with attached and cut serration configurations using CFD-based analysis.

II. Literature Review

Significant efforts have been made to understand and reduce trailing edge noise generated by airfoils. One of the foundational works in this area is the study by Brooks et al. [10], which established that trailing edge noise is primarily caused by the interaction of turbulent boundary layers with the airfoil trailing edge. Their work also provided one of the earliest prediction models for airfoil self-noise, which is still widely used as a reference.

Early investigations into noise reduction using serrations were largely experimental. Moreau and Doolan [3] demonstrated that introducing serrations at the trailing edge of a flat plate can significantly reduce broadband noise levels. Their results showed that noise reduction occurs due to the breakdown of large coherent turbulent structures into smaller, less energetic eddies. Similarly, Chong et al. [4] conducted detailed experiments on serrated airfoils and reported reductions in sound pressure levels, particularly at mid-to-high frequency ranges. They also highlighted that serration geometry plays a crucial role in determining the effectiveness of noise reduction.

With the development of numerical methods, CFD-based studies have provided deeper insight into the underlying flow physics. Kepekçi et al. [2] performed aeroacoustic simulations using the SST k-ω turbulence model combined with the Ffowcs Williams–Hawkings (FW-H) equation. Their study showed that sound pressure levels could be effectively predicted using this approach, and they identified regions near the trailing edge where maximum acoustic disturbances occur. This work demonstrated the capability of RANS-based methods in aeroacoustic prediction.

Higher-fidelity simulations have also been widely used to capture unsteady flow structures. Ji et al. [1] conducted a numerical study on a pitching NACA 0012 airfoil using Large Eddy Simulation (LES) coupled with the FW-H acoustic model. Their results showed that trailing edge serrations could reduce sound pressure levels by approximately 4 dB in certain frequency ranges, while having only a minor effect on aerodynamic performance. The study also highlighted that serrations reduce spanwise coherence and modify wake vortex structures, which contributes to noise reduction.

Further numerical investigations by Tang et al. [6] focused on the detailed mechanism of noise reduction using serrations. Using CFD and acoustic analysis, they showed that serrations reduce pressure fluctuations near the trailing edge and weaken vortex shedding intensity. Their results confirmed that the reduction in spanwise correlation of turbulent structures is a key factor in lowering acoustic emissions.

Parametric studies have also been conducted to evaluate the influence of serration geometry. Pereira et al. [7] performed a numerical analysis by varying serration amplitude and wavelength and observed that certain configurations can significantly improve noise reduction performance. Their results indicated that larger amplitudes generally lead to better noise reduction, but may also influence aerodynamic characteristics. Similarly, Gruber et al. [9] experimentally investigated different serration geometries and reported that optimized serration designs can achieve substantial reductions in broadband noise without severe aerodynamic penalties.

In addition to RANS and LES approaches, hybrid turbulence modeling techniques such as Detached Eddy Simulation (DES) have been explored. Spalart [8] introduced the DES method, which combines the advantages of RANS and LES to capture both boundary layer behavior and large-scale turbulence structures. More recent studies using hybrid CFD–acoustic methods, such as Xing et al. [11], demonstrated improved prediction of aeroacoustic characteristics by combining advanced turbulence models with FW-H formulations.

Applications of serrations have also been extended to wind turbine blades and rotating systems. Studies in this area have shown that serrations can effectively reduce broadband noise while maintaining aerodynamic efficiency, making them a practical solution for real-world applications [10].

Despite these advancements, most of the studies discussed above have focused on symmetric airfoils such as NACA 0012 and primarily considered serrations that are attached to the trailing edge. Comparatively fewer studies have investigated cambered airfoils such as NACA 2412 under steady operating conditions. In addition, limited work has been carried out on alternative serration implementations, such as cut serrations, where the trailing edge geometry is directly modified. Furthermore, there is a lack of systematic comparison between different serration configurations under identical flow conditions using consistent numerical approaches such as SST k-ω and FW-H. Therefore, there is a clear need for a detailed numerical investigation that evaluates the influence of serration configuration on both aerodynamic and aeroacoustic performance. The present study addresses this gap by analyzing a NACA 2412 airfoil at an angle of attack of 5°, incorporating sawtooth serrations at the trailing edge using the SST k-ω transient turbulence model and the Ffowcs Williams–Hawkings (FW-H) equation.

III. METHODOLOGY

Geometry Description

The present study is conducted on a three-dimensional model of the NACA 2412 airfoil, which is selected due to its well-established aerodynamic characteristics. The airfoil has a chord length of 0.1 m and is analyzed at a fixed angle of attack of 5°, representing a moderate operating condition. Although the airfoil profile is inherently two-dimensional, a finite spanwise length of 0.15C is introduced to enable realistic three-dimensional flow development and to support aeroacoustic analysis.

Two configurations are considered in this investigation. The first configuration corresponds to a baseline airfoil with a clean trailing edge, while the second configuration consists of a modified trailing edge with serrations. The serrated geometry is created using a cut-type modification, forming sharp sawtooth patterns along the trailing edge. The serrations are defined by an amplitude of 10 mm and a wavelength of 10 mm. This geometric modification is intended to alter the flow structures near the trailing edge, thereby reducing the coherence of vortex shedding and influencing the resulting aerodynamic noise.

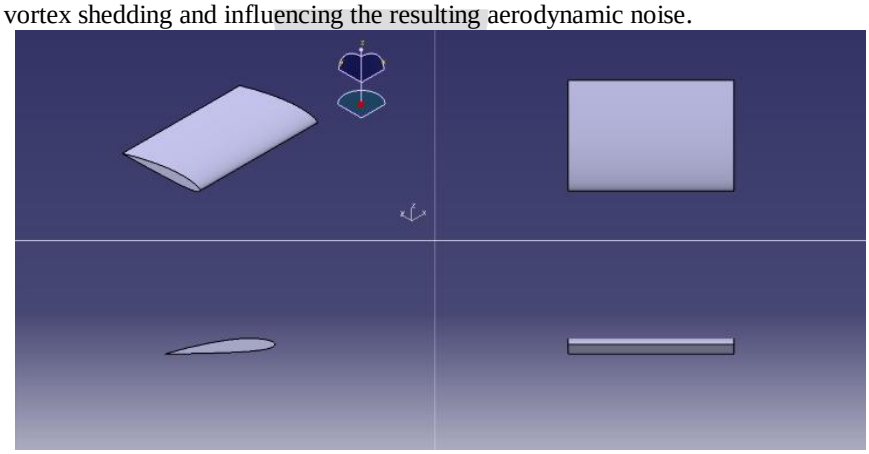

Fig. 1. Different Views of NACA 2412 wing

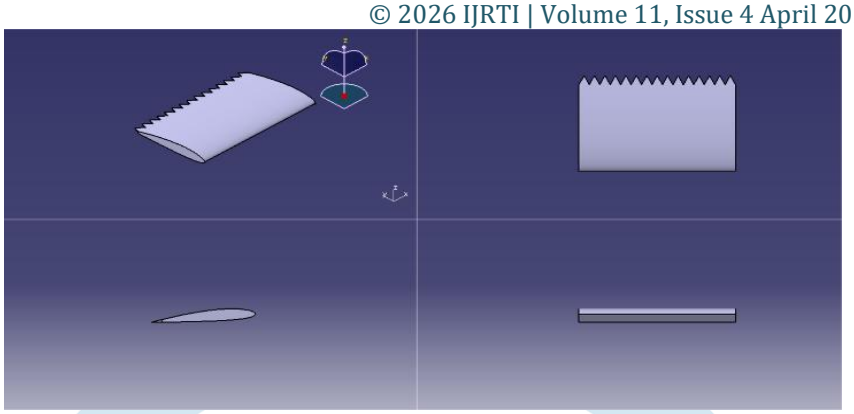

Fig. 2. Different Views of NACA 2412 Serrated Wing

Computational Domain

A three-dimensional computational domain is constructed around the airfoil to accurately capture the flow field and wake development. The domain extends to a distance of 5C upstream of the airfoil and 10C downstream, ensuring that the inflow and wake regions are sufficiently resolved without interference from the boundaries. In the spanwise direction, the domain width is maintained at 2C to allow the development of three-dimensional flow structures while maintaining computational efficiency.

The boundary conditions are defined to represent external aerodynamic flow. A uniform velocity inlet condition is applied at the upstream boundary, corresponding to a freestream velocity of 45 m/s, which yields a Reynolds number of 304,558 based on the chord length. The downstream boundary, upper, lower and front face along the span is defined as a pressure outlet with atmospheric pressure to minimize artificial reflections and confinement effects. The back face is assigned to symmetry condition, and the airfoil surface is modelled as a no-slip wall to accurately capture viscous effects.

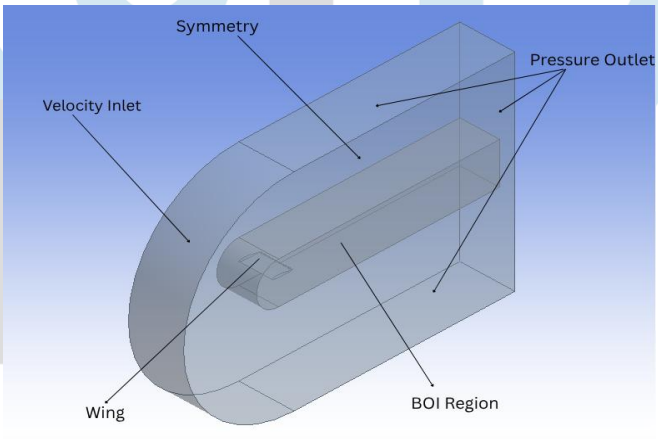

Fig. 3. Isometric view of the flow domain

Mesh Generation

The computational domain is discretized using a poly-hexacore mesh, which provides an efficient balance between accuracy and computational cost for three-dimensional simulations. This meshing approach allows better control of cell distribution in regions of interest while maintaining a manageable total cell count. The total number of cells used in the simulation is approximately 583,052 for the baseline configuration and 3,483,402 for the serrated configuration.

To achieve higher resolution in critical flow regions, a Body of Influence (BOI) is introduced around the airfoil. The BOI region extends up to 1C upstream of the leading edge and 10C downstream of the trailing edge, with a spanwise extent of 1.8C. Within this region, a finer mesh is enforced to accurately capture flow features such as boundary layer development, vortex shedding, and wake evolution. Outside the BOI region, a comparatively coarser mesh is used to reduce computational cost without significantly affecting solution accuracy.

To accurately capture near-wall effects, inflation layers are applied along the airfoil surface. A total of 10 inflation layers are used, with the first layer thickness selected to satisfy the near-wall resolution requirement. This ensures proper resolution of the viscous sublayer and enhances the accuracy of turbulence modeling using the SST k–ω model.

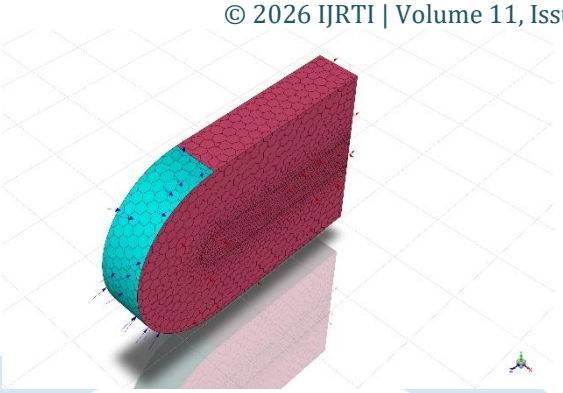

Fig. 4. Isometric view of the Mesh

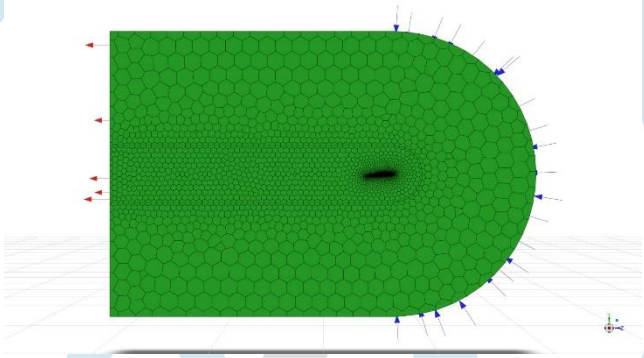

Fig. 5. Poly-hexacore mesh with BOI region near the wing

Governing Equations

The flow field is governed by the unsteady form of the Navier–Stokes equations, which represent the conservation of mass and momentum for incompressible flow. These equations are solved in a transient framework to capture time-dependent flow structures responsible for aerodynamic noise generation.

SST k /omega Turbulence Model

The SST k–ω turbulence model is a two-equation eddy viscosity model that is widely used for aerodynamic simulations due to its strong performance in predicting boundary layer behavior and separated flows. This model combines the advantages of the k–ω formulation near the wall with the k–ε behavior in the free-stream region. Because of this blending approach, it provides accurate results across the entire flow domain, from the viscous sublayer to the outer flow. It is particularly effective in handling adverse pressure gradients and flow separation, which are critical in aeroacoustic studies. However, the model may slightly overpredict turbulence levels in regions with strong normal strain, such as stagnation zones.

The formulation of the SST k–ω model begins with the transport equation for turbulent kinetic energy, which governs the evolution of turbulence intensity in the flow field:

$$\frac{\partial k}{\partial t} + U_j \frac{\partial k}{\partial x_j} = P_k - \beta^* k\omega + \frac{\partial}{\partial x_j}\left[(\nu + \sigma_k \nu_T)\frac{\partial k}{\partial x_j}\right] \tag{1}$$

Along with turbulent kinetic energy, the model also solves for the specific dissipation rate, which represents the rate at which turbulence is dissipated:

$$\frac{\partial \omega}{\partial t} + \mathrm{U_j}\frac{\partial \omega}{\partial \mathrm{x_j}} = \alpha S^2 - \beta\omega^2 + \frac{\partial}{\partial \mathrm{x_j}}\left[(\nu + \sigma_\omega \nu_T)\frac{\partial \omega}{\partial \mathrm{x_j}}\right] + 2(1 - F_1)\sigma_{\omega 2}\frac{1}{\omega}\frac{\partial k}{\partial x_j}\frac{\partial \omega}{\partial x_j} \tag{2}$$

To improve accuracy across different regions of the flow, blending functions are introduced. These functions ensure a smooth transition between near-wall and free-stream formulations. The second blending function is defined as:

$$F_2 = \tanh\left(\left[\max\left(\frac{2\sqrt{k}}{\beta^*\omega y}, \frac{500\nu}{y^2\omega}\right)\right]^2\right) \tag{3}$$

In order to prevent excessive production of turbulence in certain regions, a production limiter is applied to the turbulent kinetic energy equation:

$$P_k = \min\left(\tau_{ij}\frac{\partial u_i}{\partial x_j}, 10\beta^* k\omega\right) \tag{4}$$

The model constants are not fixed but are blended between inner and outer regions using a general blending relation:

$$\phi = \phi_1 F_1 + \phi_2(1 - F_1) \tag{5}$$

Here, the first blending function plays a key role in activating the appropriate model behavior near the wall. It is defined as:

$$F_1 = \tanh\left\{\left[\min\left(\max\left(\frac{\sqrt{k}}{\beta^*\omega y}, \frac{500\nu}{y^2\omega}\right), \frac{4\sigma_{\omega 2}k}{CD_{k\omega}y^2}\right)\right]^4\right\} \quad (6)$$

Additionally, a cross-diffusion term is included in the formulation to account for interactions between the k and ω gradients:

$$CD_{k\omega} = \max\left(2\rho\sigma_{\omega 2}\frac{1}{\omega}\frac{\partial k}{\partial x_j}\frac{\partial \omega}{\partial x_j}, 10^{-10}\right) \quad (7)$$

Using these quantities, the turbulent (eddy) viscosity is computed, which directly influences the momentum equations:

$$\nu_T = \frac{a_1 k}{\max(a_1\omega, SF_2)} \quad (8)$$

To ensure physically realistic simulations, appropriate boundary conditions must be specified. For the free-stream region, the specific dissipation rate is bounded as:

$$\frac{u_\infty}{L} < \omega_{far-field} < 10\frac{u_\infty}{L} \quad (9)$$

Similarly, the turbulent kinetic energy in the far field is constrained within the following limits:

$$10^{-5}\frac{u_\infty^2}{Re_L} < k_{far-field} < 0.1\frac{u_\infty^2}{Re_L} \quad (10)$$

At the wall, the specific dissipation rate is defined based on the near-wall grid resolution:

$$\omega_{wall} = 10\frac{6\nu}{\beta_1(\Delta d_1)^2} \quad , \quad k_{wall} = 0$$

Finally, the SST k–ω model uses a set of empirical constants, which are given as:

$$\alpha_1 = \frac{5}{9}, \quad \alpha_2 = 0.44, \quad \beta_1 = \frac{3}{40}, \quad \beta_2 = 0.0828, \quad \beta^* = 0.09$$
$$\sigma_{k1} = 0.85, \quad \sigma_{k2} = 1, \quad \sigma_{\omega 1} = 0.5, \quad \sigma_{\omega 2} = 0.856$$

FWH Acoustic Analogy

The Ffowcs Williams–Hawkings (FW-H) acoustic analogy is a well-established method used to predict sound generated by unsteady aerodynamic flows. It builds upon Lighthill's acoustic analogy by including the influence of moving solid boundaries, which makes it especially useful for studying noise from airfoils and similar configurations. In this formulation, the complex interaction between flow and sound is represented using equivalent acoustic sources distributed over a control surface and within the surrounding flow.

The FW-H equation relates the far-field acoustic pressure fluctuations to different physical noise sources, namely thickness, loading, and quadrupole contributions. The governing equation is written as:

$$\frac{1}{a_0^2}\frac{\partial^2 p'}{\partial t^2} - \nabla^2 p'(x,t) = \frac{\partial}{\partial t}[\rho_0 U_n \delta(f)] - \frac{\partial}{\partial x_i}[L_i\delta(f)] + \frac{\partial^2}{\partial x_i \partial x_j}[T_{ij}H(f)] \quad (11)$$

The first term on the right-hand side represents the monopole or thickness noise, which arises due to the displacement of fluid by the moving surface. The second term corresponds to dipole or loading noise, generated by unsteady forces acting on the surface. The final term represents quadrupole noise, which is associated with turbulent fluctuations within the flow field.

The effective velocity term used in the formulation is defined as:

$$U_i = \left(1 - \frac{\rho}{\rho_0}\right)v_i + \frac{\rho u_i}{\rho_0} \quad (12)$$

The loading term, which accounts for the forces exerted by the fluid on the surface, is expressed as:

$$L_i = [(p - p_0)\delta_{ij} - \tau_{ij} + \rho u_i(u_j - v_j)]n_j \quad (13)$$

The stress tensor term, representing the contribution from turbulent motion in the flow, is given by:

$$T_{ij} = \rho u_i u_j + [(p - p_0) - c^2(\rho - \rho_0)]\delta_{ij} - \tau_{ij} \quad (14)$$

In these expressions, p'denotes the acoustic pressure fluctuation, $\rho_0$is the ambient density, $p_0$is the ambient pressure, and $c$is the speed of sound. The Dirac delta function $\delta(f)$and the Heaviside function $H(f)$are used to distinguish between surface and volume source contributions. The vector $n_j$represents the outward normal to the integration surface, while $\tau_{ij}$is the viscous stress tensor.

After defining the source terms, the FW-H equation can be expressed in an integral form to directly compute the far-field acoustic pressure at an observer location. This formulation separates the contributions from surface and volume sources and is written as:

$$4\pi p_T'(x,t) = \int_{f=0}\left[\frac{\rho_0(U_n + u_n)}{r(1-M_r)^2}\right]_{ret} dS + \int_{f=0}\left\{\frac{\rho_0 U_n[r\dot{M}_r + c_0(M_r - M^2)]}{r^2(1-M_r)^3}\right\}_{ret} dS \quad (15)$$

Here, Mrepresents the Mach number vector at the source point, and the subscript "ret" indicates that all quantities are evaluated at the retarded time. This accounts for the finite time required for sound to propagate from the source to the observer.

To simplify the notation, several intermediate variables are introduced. The velocity components and Mach number components are defined as:

$$U_n = U_i, \dot{U}_n = \dot{U}_i n_i, M_r = M_i\hat{r}_i, \dot{M}_r = \dot{M}_i\hat{r}_i$$

Using these definitions, the FW-H equation can be further expanded into a more explicit form for practical computation:

$$4\pi p_L'(x,t) = \frac{1}{c}\int_{f=0}\left[\frac{L_r}{r(1-M_r)^2}\right]_{ret} dS + \int_{f=0}\left[\frac{L_r - L_M}{r^2(1-M_r)^2}\right]_{ret} dS + \frac{1}{c}\int_{f=0}\left[\frac{L_r\left(r\dot{M}_r + c(M_r - M^2)\right)}{r^2(1-M_r)^3}\right]_{ret} dS \tag{16}$$

where the terms $L_r$and $L_M$are defined as:

$$L_r = L_i\hat{r}_i$$
$$\dot{L}_r = \dot{L}_i + \dot{r}_i$$
$$L_M = L_i M_i$$

The contribution from quadrupole sources is further expressed using:

$$4\pi p_Q'(x,t) = \int_{f>0}\left[\frac{K_1}{c^2 r} + \frac{K_2}{cr^2} + \frac{K_3}{r^2}\right] dV \tag{17}$$

where the individual terms are given by:

$$K_1 = \frac{\ddot{T}_{rr}}{(1-M_r)^3} + \frac{\dot{M}_r T_{rr} + 3M_r\dot{T}_{rr}}{(1-M_r)^4} + \frac{3M_r^2 T_{rr}}{(1-M_r)^5}$$

$$K_2 = \frac{-\ddot{T}_{ii}}{(1-M_r)^2} - \frac{4T_{Mr} + 2\dot{T}_{Mr} + M_r T_{ii}}{(1-M_r)^3} + \frac{3[(1-M^2)T_{rr} - 2M_r T_{Mr} - M_i M_i T_{rr}]}{(1-M_r)^4} + \frac{6M_r(1-M^2)T_{rr}}{(1-M_r)^5}$$

$$K_3 = \frac{2T_{MM} - (1-M^2)T_{ii}}{(1-M_r)^3} - \frac{6(1-M^2)T_{Mr}}{(1-M_r)^4} + \frac{3(1-M^2)^2 T_{rr}}{(1-M_r)^5}$$

In these expressions, $T_{rr} = T_{ij}\hat{r}_i\hat{r}_j$ represents the double contraction of the Lighthill stress tensor, while the remaining terms describe the interaction between flow turbulence and acoustic propagation effects.

To complete the formulation, the stress tensor contractions and auxiliary terms used in the quadrupole contribution are defined as follows:

$$T_{MM} = T_{ij}M_i M_j, T_{Mr} = T_{ij}M_i\hat{r}_j, T_{Mr} = T_{ij}\dot{M}_i\hat{r}_j$$
$$\dot{T}_{Mr} = \dot{T}_{ij}M_i\hat{r}_j, T_r = T_{ij}\hat{r}_j, T_{rr} = T_{ij}\hat{r}_i\hat{r}_j, \ddot{T}_{rr} = \ddot{T}_{ij}\hat{r}_i\hat{r}_j$$

These quantities are used to represent the directional components and time variations of the Lighthill stress tensor, which are required for evaluating the quadrupole noise contribution in the FW-H formulation.

Finally, the sound pressure level (SPL) is obtained from the computed acoustic pressure fluctuations using the root mean square (RMS) value over a specified time interval. The SPL is defined as:

$$SPL = 20\log\left(\frac{p'_{rms}}{p_{ref}}\right) \tag{18}$$

where the reference pressure is given by:

$$p_{ref} = 2\times 10^{-5}\ \text{Pa}$$

IV. NUMERICAL METHOD

Solver Settings

Table 1 Solver Settings

Category	Parameter	Value
Solver	Type	Pressure-Based
	Time	Transient
Pressure-Velocity Coupling	Scheme	PISO
	Skewness Correction	2
	Neighbour Correction	1
Spatial Discretization	Gradient	Least Squares Cell-Based
	Pressure	PRESTO!
	Momentum	Second Order Upwind
	Turbulent Kinetic Energy(k)	Second Order Upwind
	Specific Dissipation Rate (ω)	Second Order Upwind
Transient Formulation	Time Integration	Second Order Implicit
Additional Settings	Warped-Face Gradient Correction	Enabled

Timestep and Convergence

The time step used in the present study is determined based on the characteristic acoustic frequency associated with the airfoil. The peak frequency of the sound generated is estimated using the Strouhal relation:

$$f_{peak} = \frac{St \times U}{L} \tag{19}$$

Taking the Strouhal number corresponding to trailing edge noise (≈ 0.1), with a freestream velocity of 45 m/s and a characteristic length of 0.01 m, the peak frequency is obtained as approximately 450 Hz. To accurately capture the acoustic waves, the maximum frequency is selected as ten times the peak frequency:

$$f_{max} = 10 f_{peak} \tag{20}$$
$$f_{max} = 4500 \approx 5000\ \text{Hz}$$

The time step is then determined by resolving the highest frequency using at least 20 time steps per cycle:

$$\Delta t = \frac{1}{20 f_{max}} \tag{21}$$
$$\Delta t = \frac{1}{20 \times 5000} = 1 \times 10^{-5}\ \text{s}$$

The convective time scale is estimated as:

$$t_c = \frac{c}{U} \tag{22}$$
$$t_c = \frac{0.1}{45} = 2.22 \times 10^{-3}\ \text{s}$$

An initial washout phase is considered to eliminate transient effects:

$$t_{washout} = 20t_c \tag{23}$$
$$t_{washout} = 0.044\,\text{s}$$

For the acoustic data acquisition, the sampling duration is determined based on the required frequency resolution:

$$\Delta f = \frac{1}{T} \tag{24}$$
$$T = \frac{1}{\Delta f}$$
$$T = \frac{1}{10} = 0.1\,\text{s}$$

This corresponds to approximately 10,000 time steps during the acoustic phase. The convergence of the numerical solution is ensured by reducing the residuals of all governing equations below 10^{-4} at each time step. In addition, key flow variables are monitored to confirm that a statistically steady state is reached before acoustic data collection begins.

Turbulence Model

The turbulence effects in the present study are modeled using the Shear Stress Transport (SST) k–ω model. This model is selected due to its strong capability in accurately predicting boundary layer behavior under adverse pressure gradients and flow separation conditions, which are critical in airfoil aeroacoustic studies.

The SST k–ω model combines the advantages of the k–ω formulation in the near-wall region with the k–ε model in the free-stream region through a blending function. This allows improved prediction of wall-bounded flows while avoiding sensitivity to free-stream turbulence levels. As a result, it provides reliable results for external aerodynamic applications involving complex flow features.

In aeroacoustic simulations, accurate resolution of unsteady flow structures is essential, as these directly influence sound generation mechanisms. The SST k–ω model has been widely adopted for such applications due to its ability to capture shear layer development and separation phenomena with good accuracy.

A similar approach has been employed by H. Kepekçi et al. [2], where computational aeroacoustic analysis of airfoils was performed using CFD methods. Their study highlights the suitability of turbulence modeling techniques in predicting unsteady flow behavior associated with aerodynamic noise generation.

Therefore, the SST k–ω model is considered appropriate for the present investigation due to its balance between computational efficiency and accuracy in capturing flow features relevant to aeroacoustic predictions.

Acoustic Model

The aeroacoustic analysis in the present study is performed using the Ffowcs Williams–Hawkings (FW-H) acoustic analogy, which enables the prediction of radiated sound from unsteady flow fields by transforming flow variables into equivalent acoustic source terms.

In this work, the airfoil surface is employed directly as the FW-H source surface, corresponding to an impermeable formulation. This approach captures the dominant dipole-type noise associated with unsteady pressure loading on the airfoil surface, which is the primary mechanism responsible for trailing edge noise generation in low Mach number flows.

The acoustic pressure at a far-field observer location is expressed as:

$$p'(x,t) = p'_T + p'_L + p'_Q \tag{25}$$

where p'_T, p'_L, and p'_Q denote the thickness, loading, and quadrupole contributions, respectively. For the present case, the loading noise component is expected to dominate due to boundary layer interaction at the trailing edge.

A total of five acoustic receivers are positioned strategically to capture both near-field and far-field acoustic characteristics. The chord length of the airfoil is $c = 0.1$ m. Two receivers are placed at a distance of $0.1c$ downstream of the trailing edge, one at the mid-span and the other near the wing tip. These locations are selected to capture the immediate acoustic signature of trailing edge noise, which is generated by the interaction of turbulent boundary layer structures with the sharp trailing edge.

To evaluate the propagation of acoustic waves into the far-field, additional receivers are placed at $9c$ downstream of the trailing edge at corresponding spanwise locations (mid-span and wing tip). These receivers capture the radiated sound after spatial

development, allowing assessment of far-field noise characteristics. An additional receiver is positioned near the wing tip in the upper region to account for three-dimensional effects and directional variation in acoustic radiation.

The acoustic signals are recorded as time-resolved pressure fluctuations at each receiver location. The simulation is performed for a total duration of 0.15 s, ensuring sufficient temporal data for spectral analysis.

The recorded pressure signals are post-processed to obtain the Sound Pressure Level (SPL), defined as:

$$SPL = 20 \log\left(\frac{p'_{rms}}{p_{ref}}\right) \tag{26}$$

where p'_{rms} is the root mean square value of the fluctuating pressure signal and p_{ref} is the reference pressure.

The frequency-domain characteristics of the acoustic signal are obtained using Fast Fourier Transform (FFT), enabling identification of dominant tonal and broadband noise components associated with trailing edge vortex shedding and turbulent boundary layer interactions

Table 2 Receiver Locations

Name	X-Coord.(m)	Y-Coord.(m)	Z-Coord.(m)
Receiver-1	0	-0.008715574	-0.09962947
Receiver-2	0.15	-0.008715574	-0.09962947
Receiver-3	0	-0.008715574	-0.99962947
Receiver-4	0.15	-0.008715574	-0.99962947
Receiver-5	0.15	0.15875574	-0.99962947

V. RESULTS

Aerodynamic results

The drag coefficient variation with flow time shows a clear transient followed by steady convergence for both configurations. Initially, the drag rises rapidly from about Cd ≈ 0.02 to a peak of approximately 0.074–0.075 (serrated) and 0.072–0.073 (baseline) at around $t \approx 0.015–0.02$. After this overshoot, both cases settle to nearly constant values. The steady-state drag is approximately Cd ≈ 0.071 for the baseline and slightly higher at Cd ≈ 0.072 for the serrated case, indicating a very small drag penalty due to serrations.

The lift coefficient follows a similar transient pattern. The lift increases sharply from near zero to a peak of about Cl ≈ 0.70 (baseline) and Cl ≈ 0.68–0.69 (serrated) at $t \approx 0.015$. This is followed by a small drop and stabilization. In steady state, the baseline maintains a lift of approximately Cl ≈ 0.665–0.67, while the serrated case stabilizes slightly lower at Cl ≈ 0.65–0.655. This shows a minor reduction in lift due to the serrated trailing edge.

The pressure coefficient distribution along the chord provides further insight into the flow behavior. Near the leading edge ($x/c < 0.01$), both cases exhibit a strong suction peak reaching about Cp ≈ 2.4–2.5. Moving downstream, the pressure rapidly decreases and then oscillates along the chord. In the mid-chord region ($x/c \approx 0.02–0.08$), the Cp values fluctuate roughly between 0.1 and 1.1 for both cases, but the serrated configuration shows slightly larger and more irregular oscillations.

Towards the trailing edge ($x/c \approx 0.1$), both cases show pressure recovery, reaching approximately Cp ≈ 1.2–1.25. However, the serrated case exhibits a less smooth recovery with more visible fluctuations, indicating increased local flow disturbances.

Overall, the quantitative comparison shows that the serrated trailing edge results in:

- A small increase in steady drag (~0.001 higher Cd),
- A slight reduction in lift (~0.01–0.015 lower Cl),
- Increased pressure fluctuations along the chord.

These trends suggest that while serrations introduce additional flow mixing and unsteadiness, their impact on global aerodynamic performance remains relatively small.

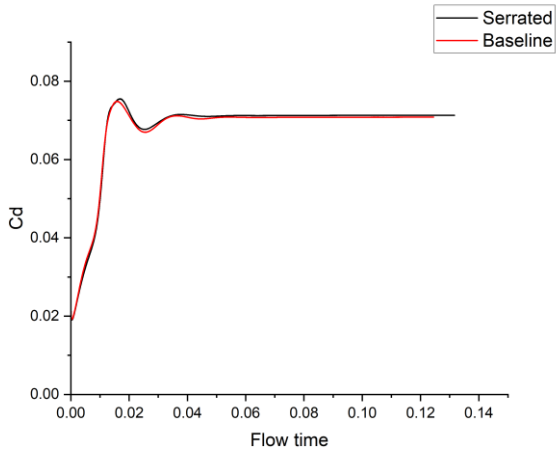

Fig. 6. Cd variation for Baseline and Serrated NACA 2412 wing

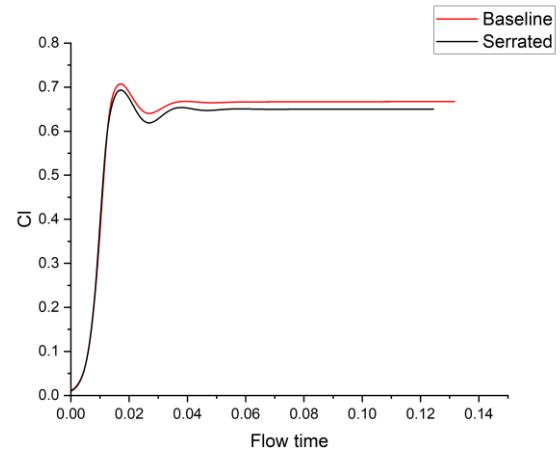

Fig. 7. Cl variation for Baseline and Serrated NACA 2412 wing

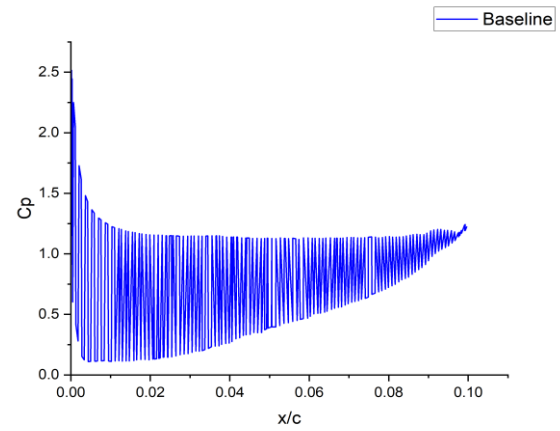

Fig. 8. Cp distribution for Baseline NACA 2412 wing at 5 deg AOA

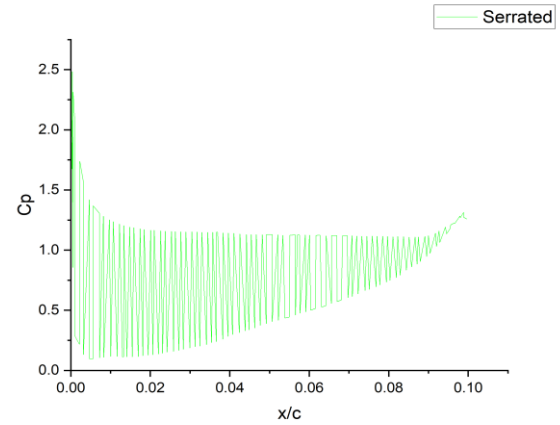

Fig. 9. Cp distribution for Serrated NACA 2412 wing at 5 deg AOA

Acoustic Results

The sound pressure level (SPL) variation with frequency shows a clear broadband decay trend for all receiver locations. At low frequencies (around 20–50 Hz), the SPL values are relatively high, especially for receivers closer to the trailing edge. For instance, Receiver 1 (baseline) records about 46–47 dB at 20 Hz, which gradually decreases to approximately 20 dB at 500 Hz. A similar trend is observed for the serrated case, but with consistently lower SPL values.

Across all receivers, the serrated trailing edge results in a noticeable reduction in noise levels. At low frequencies, the reduction is modest, typically around 1–3 dB. For example, at 50 Hz, Receiver 1 shows approximately 42 dB (baseline) compared to ~39–40 dB (serrated). As the frequency increases, the noise reduction becomes slightly more consistent, with differences of about 2–4 dB observed across most receivers.

The effect of receiver position is also evident. Receivers placed closer to the trailing edge (e.g., Receiver 1 and Receiver 2) record higher SPL values, while downstream receivers (Receiver 4 and Receiver 5) show significantly lower levels. For instance, at 100 Hz, Receiver 5 records around −5 to −7 dB (baseline), whereas Receiver 1 is still above 30 dB. This confirms the decay of acoustic intensity with distance from the primary noise source.

The 1/3 octave band analysis further clarifies the frequency-dependent behavior. In this representation, the baseline case shows peak SPL values around 50–52 dB at 63–80 Hz for Receiver 1, while the serrated case reduces this to approximately 46–48 dB. Similarly, for Receiver 2, the SPL decreases from about 47 dB (baseline) to ~43–44 dB (serrated) in the same frequency band.

At mid frequencies (160–315 Hz), the SPL values gradually reduce. For example, Receiver 1 drops to about 42–43 dB (baseline) and ~39–40 dB (serrated). At higher frequencies (400–500 Hz), the SPL further decreases to around 40 dB (baseline) and ~36–37 dB (serrated).

For receivers located farther downstream, the SPL values are much lower overall. Receiver 5 shows values around 10–12 dB (baseline) at low frequencies, decreasing to near 0 to −1 dB at higher frequencies, while the serrated case consistently reduces these levels by about 2–3 dB.

Overall, the acoustic results indicate that the serrated trailing edge provides a consistent broadband noise reduction, typically in the range of 2–4 dB across most frequencies and receiver locations. The reduction is more noticeable in the low-to-mid frequency range, which is characteristic of trailing-edge noise. These observations confirm that the serrations effectively disrupt coherent vortex shedding and reduce acoustic radiation without significantly altering the overall frequency trend.

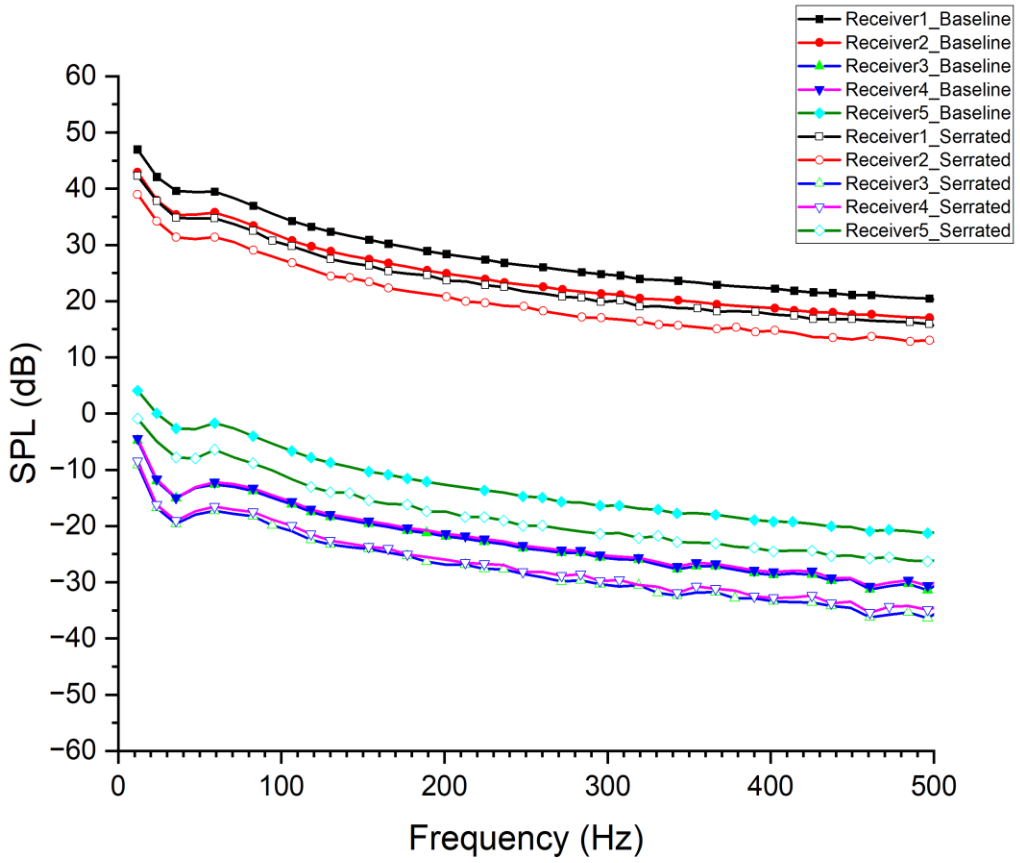

Fig. 10. SPL vs Frequency for both Baseline and Serrated NACA 2412 wing

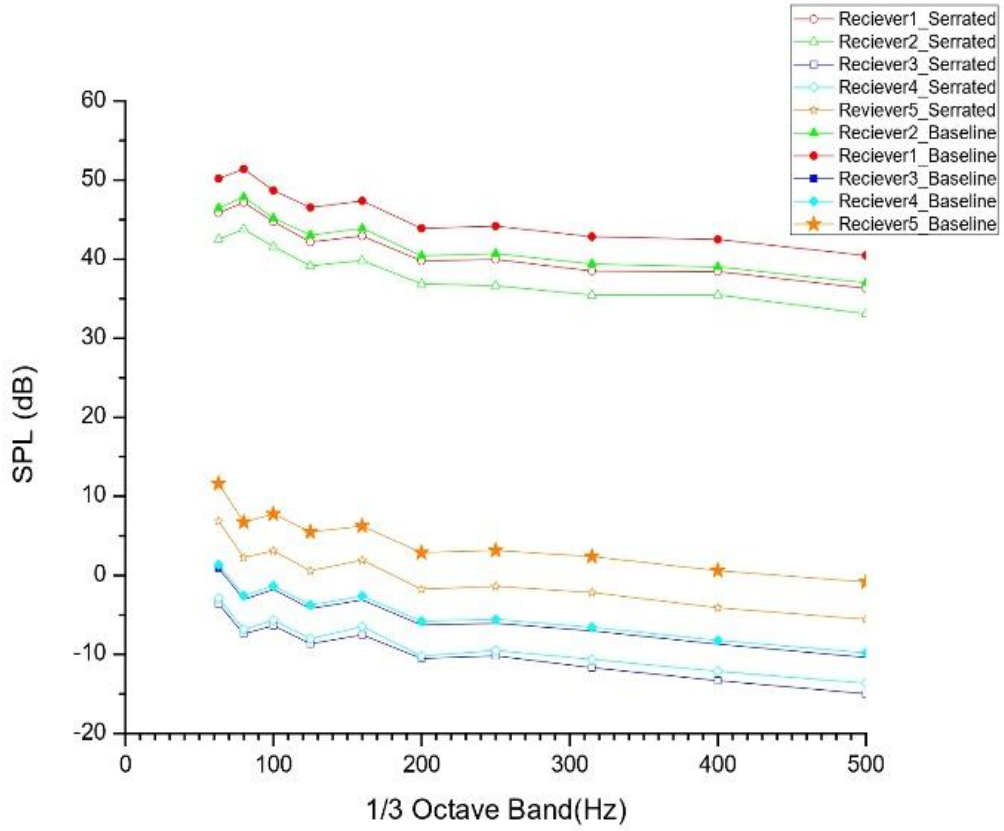

Fig. 11. SPL vs 1/3 octave for both Baseline and Serrated NACA 2412 wing

Flow field Contours

The velocity contours of the baseline configuration show a clear acceleration of flow over the upper surface of the airfoil, with peak velocities reaching approximately 85–90 m/s near the leading edge. A low-velocity region is observed at the leading edge stagnation point, followed by a smooth development of the wake downstream. The wake region behind the trailing edge appears relatively coherent and narrow, indicating organized flow structures.

In contrast, the serrated configuration exhibits a slightly altered velocity distribution near the trailing edge. While the overall acceleration over the airfoil remains similar, the wake region becomes more diffused and elongated. The velocity contours indicate increased mixing in the downstream region, with a less coherent wake structure compared to the baseline case. This suggests that the serrations disturb the flow and promote enhanced momentum exchange.

The static pressure contours further support these observations. For the baseline airfoil, a high-pressure region is clearly visible at the leading edge, followed by a gradual pressure drop over the upper surface and recovery toward the trailing edge. The pressure field appears smooth and well-organized, indicating stable flow behavior.

For the serrated configuration, the overall pressure distribution remains similar near the leading edge, with a comparable high-pressure stagnation region. However, near the trailing edge, slight irregularities in the pressure contours can be observed. The pressure recovery is less uniform, and small localized variations appear in the wake region. These variations indicate the presence of disturbed flow structures introduced by the serrations.

Overall, the contour analysis shows that while the leading-edge behavior remains largely unaffected, the trailing edge geometry significantly influences the downstream flow. The serrated trailing edge disrupts the coherence of the wake, increases mixing, and introduces small-scale variations in both velocity and pressure fields. These changes are consistent with the observed reduction in acoustic emissions, as the breakdown of organized flow structures reduces the strength of noise-generating mechanisms.

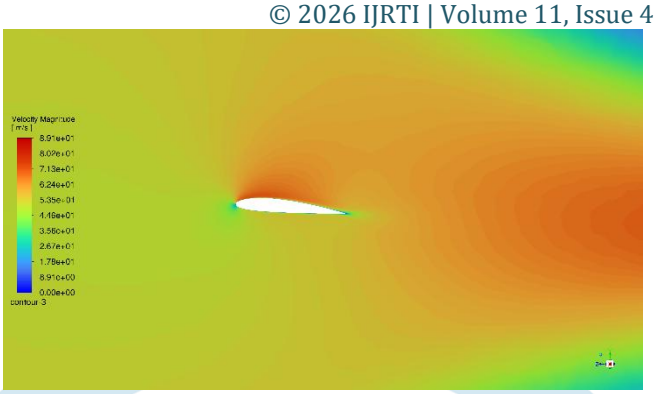

Fig. 12. Velocity Contour for NACA 2412 Baseline wing

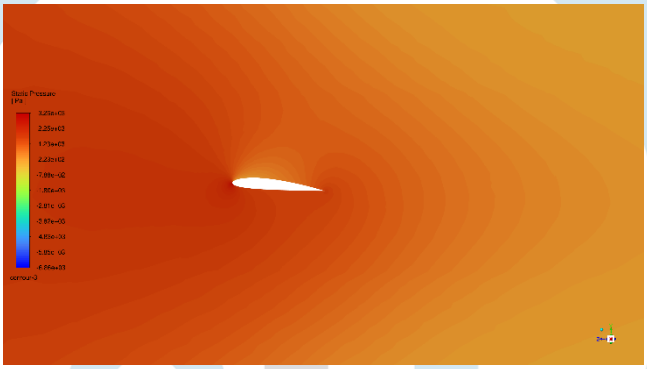

Fig. 13. Static Pressure Contour for NACA 2412 Baseline wing

Fig. 14. Static Pressure Contour for NACA 2412 Serrated wing

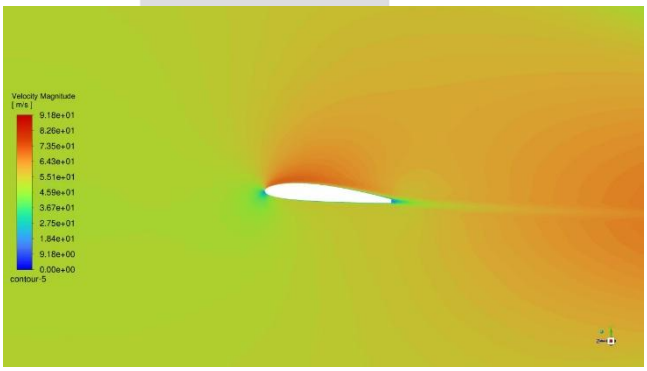

Fig. 15. Velocity Contour for NACA 2412 Serrated wing

VI. CONCLUSION

This study investigated the aerodynamic and aeroacoustic effects of trailing edge serrations on a NACA 2412 airfoil using a CFD-based approach. The results show that while the serrated configuration introduces a slight aerodynamic penalty, with a small increase in drag and a marginal reduction in lift, the overall impact on aerodynamic performance remains limited.

In contrast, the aeroacoustic analysis demonstrates a clear benefit of serrations, with consistent broadband noise reduction observed across all receiver locations and frequency ranges. The reduction is more evident in the low-to-mid frequency range, confirming the effectiveness of serrations in weakening coherent turbulent structures near the trailing edge.

Overall, the study highlights that trailing edge serrations provide a practical and efficient passive solution for noise reduction, achieving noticeable acoustic improvements without significantly affecting aerodynamic characteristics.

REFERENCES

[1] X. Ji, L. Wang, S. Ravi, J. Young, J. C. S. Lai, and F.-B. Tian, "Aerodynamic and aeroacoustic performance of a pitching foil with trailing edge serrations," *Theoretical and Computational Fluid Dynamics*, vol. 38, pp. 825–844, 2024.

[2] H. Kepekçi, B. Zafer, and H. R. Güven, "Aeroacoustics investigations of unsteady 3D airfoil for different angle using computational fluid dynamics software," *International Journal of Mechanical and Mechatronics Engineering*, vol. 12, no. 8, pp. 813–815, 2018.

[3] S. Moreau and C. J. Doolan, "Noise-reduction mechanism of a flat-plate serrated trailing edge," *AIAA Journal*, vol. 51, no. 10, pp. 2513–2522, 2013.

[4] T. P. Chong, A. Vathylakis, P. F. Joseph, and M. Gruber, "On the aeroacoustic and flow structures developed on a flat plate with a serrated trailing edge," *Journal of Sound and Vibration*, vol. 332, no. 24, pp. 6335–6358, 2013.

[5] J. E. Ffowcs Williams and D. L. Hawkings, "Sound generation by turbulence and surfaces in arbitrary motion," *Philosophical Transactions of the Royal Society A*, vol. 264, no. 1151, pp. 321–342, 1969.

[6] Y. Tang, X. Liu, and Z. Sun, "Numerical investigation of aeroacoustic noise reduction using trailing edge serrations," *Applied Sciences*, vol. 9, no. 18, p. 3784, 2019.

[7] M. Pereira, J. Catalano, and R. V. Oliveira, "Parametric study of serration geometry on aeroacoustic performance," *Applied Acoustics*, vol. 206, 2023.

[8] P. R. Spalart, "Detached-eddy simulation," *Annual Review of Fluid Mechanics*, vol. 41, pp. 181–202, 2009.

[9] A. Gruber, T. P. Chong, and P. F. Joseph, "Trailing edge serrations for broadband noise reduction," *Journal of the Acoustical Society of America*, vol. 136, no. 3, pp. 1142–1153, 2014.

[10] T. F. Brooks, D. S. Pope, and M. A. Marcolini, *Airfoil self-noise and prediction*, NASA Reference Publication, 1989.

[11] Z. Xing, H. Liu, and Y. Zhang, "Aeroacoustic prediction using hybrid CFD and FW-H methods," *Aerospace*, vol. 10, no. 4, 2023.